Carbohydrate Polymers 186 (2018) 110–121

Contents lists available at ScienceDirect

Carbohydrate Polymers

journal homepage: www.elsevier.com/locate/carbpol

Nanostructured electrospun nonwovens of poly(ε-caprolactone)/quaternized chitosan for potential biomedical applications

Danilo Martins dos Santos[a], Ilaiáli Souza Leite[b], Andrea de Lacerda Bukzem[a], Rachel Passos de Oliveira Santos[a], Elisabete Frollini[a], Natalia Mayumi Inada[b], Sérgio Paulo Campana-Filho[a,*]

[a] Sao Carlos Institute of Chemistry/University of Sao Paulo, Av. Trabalhador sao-carlense, 400–13566-590, Sao Carlos, São Paulo, Brazil
[b] Sao Carlos Institute of Physics/University of São Paulo, PO Box 369, 13560-970, Sao Carlos, Sao Paulo, Brazil

ARTICLE INFO

Keywords:
Electrospinning
Quaternized chitosan
Biomaterial
Nonwoven
Nanofibers
Wound dressing

ABSTRACT

Blend solutions of poly(ε-caprolactone) (PCL) and *N*-(2-hydroxy)-propyl-3-trimethylammonium chitosan chloride (QCh) were successfully electrospun. The weight ratio PCL/QCh ranged in the interval 95/5–70/30 while two QCh samples were used, namely QCh1 ($\overline{DQ}$ = 47.3%; $\overline{DPv}$ = 2218) and QCh2 ($\overline{DQ}$ = 71.1%; $\overline{DPv}$ = 1427). According to the characteristics of QCh derivative and to the QCh content on the resulting PCL/QCh nonwoven, the nanofibers displayed different average diameter (175 nm–415 nm), and the nonwovens exhibited variable porosity (57.0%–81.6%), swelling capacity (175%–425%) and water vapor transmission rate (1600 g m^{-2} 24 h–2500 g m^{-2} 24 h). The surface hydrophilicity of nonwovens increases with increasing QCh content, favoring fibroblast (HDFn) adhesion and spreading. Tensile tests revealed that the nonwovens present a good balance between elasticity and strength under both dry and hydrated state. Results indicate that the PCL/QCh electrospun nonwovens are new nanofibers-based biomaterials potentially useful as wound dressings.

1. Introduction

Skin is a multifunctional organ responsible for providing sensation, thermo-regulation and physical protection, and for playing metabolic and immune functions (Abrigo, McArthur, & Kingshott, 2014). Injuries caused by trauma, surgery, burn or chronic diseases may damage the skin integrity, affecting the homeostasis and exposing the body to possible infections (Song et al., 2016). Depending on the size and extent of the wound, skin can heal itself, but in case of a serious injury that provokes the lost of large area of skin, dressing the wound is required (Abrigo et al., 2014; Shevchenko, James, & James, 2009). An ideal wound dressing should be convenient for handling, applying and painless to remove, and it should provide protection for the injured site from contamination, maintain an adequate moist wound environment, allow gas exchange and accelerate the healing process (Boateng, Matthews, Stevens, & Eccleston, 2008; MacNeil, 2007; Mele, 2016). Nonetheless, although a diversified range of wound dressings is currently available, few among the available materials can satisfactorily fulfill these multiple purposes.

Electrospun polymeric micro/nanofibrous nonwovens have been widely investigated for wound dressing applications. These fibrous dressings may closely resemble the architecture of the extracellular matrix (ECM), which may serve as a template for skin cells proliferation, and hence stimulate tissue regeneration (Mele, 2016). The inherent high porosity and surface area to volume ratio exhibited by electrospun fiber matrices are beneficial for exuding fluid from the wound, transport of nutrients to cell, and gas permeation (Hassiba et al., 2016; Mele, 2016; Rieger, Birch, & Schiffman, 2013). Additionally, electrospun nonwovens are flexible, thereby allowing high conformability to the wound site, and providing an effective physical barrier to protect the wound from further physical damages and contaminations from exogenous microorganisms (Abrigo et al., 2014; Liakos et al., 2015).

A broad range of synthetic and natural polymers as well as polymer blends have been successfully electrospun. Polycaprolactone (PCL), a semicrystalline and hydrophobic aliphatic polyester composed of hexanoate repeating units, has been widely electrospun either alone or in combination with other synthetic or natural polymers to fabricate micro/nanofibrous nonwovens for wound healing applications (Cipitria, Skelton, Dargaville, Dalton, & Hutmacher, 2011; Labet & Thielemans, 2009). Despite PCL nonwoven be biocompatible and exhibit mechanical properties similar or superior to those presented by

* Corresponding author.
E-mail addresses: danilo_martins@usp.br (D.M. dos Santos), ilaiali.leite@usp.br (I.S. Leite), andreabukzem@usp.br (A.d.L. Bukzem), rachelpassos@usp.br (R.P. de Oliveira Santos), elisabete@iqsc.usp.br (E. Frollini), nataliainada@ifsc.usp.br (N.M. Inada), scampana@iqsc.usp.br (S.P. Campana-Filho).

https://doi.org/10.1016/j.carbpol.2018.01.045
Received 28 September 2017; Received in revised form 9 January 2018; Accepted 13 January 2018
Available online 31 January 2018
0144-8617/

human skin, its hydrophobic nature is strongly harmful for maintaining an adequate moist wound environment and for favoring cell adhesion, hindering the healing process (Ghasemi-Mobarakeh, Prabhakaran, Morshed, Nasr-Esfahani, & Ramakrishna, 2008).

N-(2-hydroxy)-propyl-3-trimethylammonium chitosan chloride (QCh) is a quaternized derivative of chitosan synthesized by reacting glycidyltrimethylammonium chloride (GTMAC) and chitosan (Ch) that displays interesting properties aiming its application to elaborate biomaterials, such as hydrophilicity, nontoxicity, biodegradability, biocompatibility, mucoadhesiviness, antimicrobial activity and moisture retention capacity (Prado & Matulewicz, 2014; Sonia & Sharma, 2011; Xu, Du, Huang, & Gao, 2003). These properties make this derivative a potential candidate for the design of wound dressing materials. However, attempts to electrospin solutions of quaternized chitosan derivatives were unsuccessful due to the higher repulsive forces between ionogenic groups and, consequently, a significant fraction of a nonionic polymer, such as poly(L-lactide-*co*-d, L-lactide) or poly(vinyl alcohol), was required to render the solution electrospinnable (Alipour, Nouri, Mokhtari, & Bahrami, 2009; Ignatova et al., 2010; Ignatova, Manolova, & Rashkov, 2007).

Considering the aforementioned limitations of polycaprolactone and quaternized chitosan derivative, the rational of this study is the blending of these polymers aiming to produce a superior material that combines the benefits of both, displaying tissue compatibility and improved mechanical properties. To our knowledge, there has been no report on electrospinning of polycaprolactone (PCL)/*N*-(2-hydroxy)-propyl-3-trimethylammonium chitosan chloride (QCh) blend. In this study, two samples of *N*-(2-hydroxy)-propyl-3-trimethylammonium chitosan chloride possessing different characteristics, *i.e.* average degree of quaternization ($\overline{DQ}$) and viscosity average degree of polymerization ($\overline{DPv}$), were synthesized, blended with PCL in acetic acid/formic acid (60/40 v/v) and electrospun into fibrous nonwovens intended to be applied as wound dressings. The PCL/QCh nonwovens were characterized in terms of morphology, surface properties, water absorption capacity, moisture permeation and tensile properties. *In vitro* experiments were carried out to evaluate the susceptibility of PCL/QCh nonwovens to enzymatic degradation, cytotoxicity toward neonatal human dermal fibroblasts (HDFn) and cell adhesion.

2. Material and methods

2.1. Materials

Formic acid (85.0%) and acetic acid (99.8%) were acquired from Synth (Diadema/SP; Brazil) while poly(ε-caprolactone) (PCL, Mn ≈ 80.000 g mol^{-1}),glycidyltrimethylammonium chloride (GTMAC), MTT (MTT (3-[4,5-dimethylthiazol-2-yl]-2,5- diphenyltetrazolium bromide)) and hexamethyldisilazane (HMDS) were purchased from Sigma-Aldrich (Saint Louis, MO; USA) and all of them were used as received. Glutaraldehyde was purchased from Merk KGaA (Darmstadt, Germany). Commercial chitosan (Cheng Yue Planting Co Ltd, China) was dissolved in 1% aqueous acetic acid solution to result in Cp = 3 g L^{-1}, the resulting solution was filtered through 0.45 mm membrane (Millipore®), and then it was neutralized by addition of 1 mol L^{-1} NaOH solution to induce the precipitation of chitosan. The solid was thoroughly washed with distilled water and with ethanol/water mixtures of increasing ethanol content (70%, 80%, 90%). The purified chitosan was then dried at 30 °C and the degree of deacetylation ($\overline{DD}$) of chitosan was 95% as determined by ^{1}H NMR analysis (Santos, Bukzem, & Campana-Filho, 2016). The viscosity average molecular weight ($\overline{M_v}$) of purified chitosan was determined from intrinsic viscosity measurements in 0.3 mol L^{-1} acetic acid/0.2 mol L^{-1} sodium acetate buffer (pH 4.5) at 25.00 ± 0.01 °C by using the Mark–Houwink–Sakurada equation, resulting in $\overline{Mv}$ ≈ 85.000 g mol^{-1}(Rinaudo, Milas, & Dung, 1993; Santos et al., 2016).

Neonatal human dermal fibroblast cell line (HDFn, Gibco®, cat. n° C0045C) was purchased from Thermo Fischer Scientific (Waltham, MA, USA). The cells were tested between passages 15 and 20 and were grown continuously in humidified incubator (MCO-17AC, Sanyo Electric Co. Ltd., Osaka, Japan) at 37 °C and 5% CO_2 atmosphere with Dulbecco's Modified Eagle Medium (DMEM) supplemented with 10% (v/v) fetal bovine serum (FBS) and 0.5% (v/v) penicillin-streptomycin, all purchased from Cultilab (Campinas, SP, Brazil).

2.2. Synthesis of N-(2-hydroxy)-propyl-3-trimethylammoniumchitosan chloride (QCh)

N-(2-hydroxy)-propyl-3-trimethylammoniumchitosan chloride (QCh) was synthesized by reacting glycidyltrimethylammonium chloride (GTMAC) and chitosan (Ch) in acid medium under microwave irradiation according as reported in the literature (Santos et al., 2016). In brief, purified chitosan (0.5 g) was suspended in 30 mL of deionized water and 150 μL of glacial acetic acid were added to the suspension, which was kept at constant stirring for 10 min at room temperature. Then, an aqueous solution of GTMAC was added dropwise to the chitosan suspension, which was submitted to microwave irradiation at a power of 200 W in a monomode microwave reactor (Discover-LabMate, CEM, USA) under constant stirring at the desired temperature and during a given time. Acetone excess was then added to the reaction medium to result in product precipitation, which was filtered, thoroughly washed with acetone and dried at 35 °C for 24 h. Aiming to produce two QCh samples possessing different average degree of quaternization ($\overline{DQ}$), the microwave-assisted synthesis was carried out by using the following reaction conditions: *i*) sample QCh1: molar ratio GTMAC/chitosan = 4/1, reaction time = 20 min, reaction temperature = 75 °C; *ii*) sample QCh2: molar ratio GTMAC/chitosan = 6/1, reaction time = 30 min, reaction temperature = 85 °C. The average degree of quaternization ($\overline{DQ}$) was calculated by treating the ^{1}H NMR spectra according to the method described in a previous work(Santos et al., 2016), resulting in $\overline{DQ}$ = 47.3 ± 0.4% and $\overline{DQ}$ = 71.1 ± 0.8% for samples QCh1 and QCh2, respectively. The intrinsic viscosity of QCh1 and QCh2 derivatives was determined in 0.3 mol L^{-1} acetic acid/0.2 mol L^{-1} sodium acetate buffer (pH 4.5) at 25.00 ± 0.01 °C, resulting in [η] = 288 ± 3 mL g^{-1} and [η] = 233 ± 3 mL g^{-1}, respectively (Santos et al., 2016). The viscosity average molecular weight of both derivatives was calculated from the respective intrinsic viscosity by using the Mark-Houwinck-Sakurada parameters reported in the literature (Yevlampieva, Gubarev, Gorshkova, Okrugin, & Ryumtsev, 2015) and, taking into account their average degrees of quaternization, the viscosity average degree of polymerization ($\overline{DPv}$) of QCh1 and QCh2 were calculated as $\overline{DPv}$ = 2218 e $\overline{DPv}$ = 1427, respectively. (Santos et al., 2016)

2.3. Electrospinning process

Polymer solutions (Cp = 14% w/v) were prepared by dissolving PCL and QCh at weight ratios of 100/0, 95/5, 90/10; 80/20 and 70/30 in acetic acid and formic acid solution (60/40 v/v) upon stirring for 3 h at room temperature. The conductivity of the spinning solution was determined by a conductivity meter (Gehaka, model CG 1800) at 25.0 ± 0.2 °C while its dynamic viscosity (μ, cP) was measured by using a falling-ball viscometer (GILMONT instruments) at 25.0 ± 0.2 °C and was calculated according to Eq. (1).

$$\mu = K(\rho_{ball} - \rho_{solution})t \quad (1)$$

where ρ_{ball} = density of tantalum ball (16.6 g cm^{-3}); $\rho_{solution}$ = density of spinning solution (g cm^{-3}); t = time of descent of ball (min.); K = viscometer constant (37).

The electrospinning solution was loaded into a 1 mL syringe coupled to a syringe pump, which was set to deliver the solution through a 27 gauge metallic needle (0.45 mm in diameter) at constant flow rate

(15 μL/min). A voltage of 25 kV was applied by using a digital Electrospinning Apparatus EC-DIG (IME Technologies, Geldrop, Netherlands). A stainless-steel rotating drum collector (L = 12.5 cm, W = 5.5 cm, INSTOR Projetos e Robótica Ltda, Porto Alegre/RS, Brazil) was placed at 15 cm from the needle tip and rotated at ≈2500 rpm for fiber collection. All experiments were carried out during 40 min at 25 ± 2 °C and 60 ± 5% relative humidity. After electrospinning, the resulting nonwoven was carefully removed from the drum collector, dried at 30 °C for 12 h and stored in a desiccator.

2.4. Characterization

2.4.1. Nonwoven morphology

Morphology observations of PCL/QCh nonwovens were carried out by using a LEO-440 scanning electron microscope (SEM; Leica Microsystems, Wetzlar, Germany) at an acceleration voltage of 20 kV after sputter coating with gold (JEOL JFC-1600, JEOL Ltd. DATUM Solution Business Operations, Tokyo, Japan). The fibers average diameter was determined from the SEM images by using ImageJ 1.45 software (National Institutes of Health, Bethesda, MD, USA), measuring at least 150 random fibers from 4 micrographs for each nonwoven while the fibers orientation was evaluated with OrientationJ, a plugin of ImageJ. At least four images per sample were used to evaluate the alignment of the nanofibers, quantitatively expressed by the coherency coefficient, the closer to 1 (0) the more aligned (randomly oriented) the fibers.

2.4.2. Porosity measurement

The porosity of the nonwovens was measured by the liquid displacement method(Liang, Lu, Yang, Gao, & Chen, 2016) employing absolute ethanol as the displacement liquid, since it is a non-solvent for PCL and QCh that permeates through the pores, causing negligible swelling or shrinkage. Thus, a dry sample characterized by its weight (w_1) and volume (V) was immersed in ethanol, and then a series of evacuation-repressurization cycles were carried out to force the ethanol into the pores of the nonwoven until no air bubbles emerged from it. Following, the weight (w_2) of the sample saturated with ethanol was measured and the porosity was calculated by using Eq. (2). The experiment was carried out in quadruplicate.

$$\text{Porosity}(\%) = \left(\frac{w_2 - w_1}{V\rho_{\text{ethanol}}}\right)x100 \quad (2)$$

where $\rho_{\text{ethanol}} = 0.789\ g/cm^3$

2.4.3. Attenuated total reflectance fourier transform infrared spectroscopy

ATR-FTIR spectra of electrospun nonwovens were recorded on a PerkinElmer Spectrum frontier spectrometer by using a universal attenuated total reflection (ATR) accessory (diamond/ZnSe crystal). Spectra were recorded between 4000 and 600 cm^{-1} by the accumulation of 32 scans with a resolution of 4 cm^{-1}.

2.4.4. Contact angle, surface and interfacial free energy

Contact angle (CA) measurements were carried out by using a goniometer (CAM 2008, KSV) equipped with CAM 2008 software. Nonwovens strips (10 mm x 10 mm) were attached to glass slides to maintain a horizontal surface and apparent contact angles were determined from the sessile profile droplets (approx. 5 μL) of three pure liquids of different polarities, namely deionized water, diiodomethane and ethylene glycol, 1 s after deposition. Nonwoven surface free energy and surface energy components were calculated from contact angle (CA) data and the surface tension components of the probe liquids (γ_L, γ_L^{LW}, γ_L^-, γ_L^+) (Rojo et al., 2015) by using the using the Young's equation in the form of Eq. (3), as proposed by van Oss, Chaudhery and Good model (Van Oss, Chaudhury, & Good, 1988).

$$(1 + \cos\theta)\gamma_L = 2(\sqrt{\gamma_S^{LW}\gamma_L^{LW}} + \sqrt{\gamma_S^+\gamma_L^-} + \sqrt{\gamma_S^-\gamma_L^+}) \quad (3)$$

where θ is the contact angle, γ_L is the total surface tension of the liquid, γ^{LW} is the apolar component, also named Lifshitz-van der Waals component, γ^+ is the electron acceptor component, γ is the electron donor component and the subscripts "S" and "L" denote the solid and liquid phases, respectively.

According to van Oss, Chaudhery and Good model, the total surface energy (γ^{TOTAL}) is the sum of the apolar (γ^{LW}) and polar (γ^{AB}) components ($\gamma^{TOTAL} = \gamma^{LW} + \gamma^{AB}$), the latter being calculated from γ^+ and γ (Eq. (4)).

$$\gamma^{AB} = 2(\sqrt{\gamma_S^+\gamma_S^-}) \quad (4)$$

A quantitative measure of the hydrophobicity (hydrophilicity) of surface nonwovens was assessed from the interfacial free energy (ΔG), which was determined from surface energy components of nonwovens (γ_S^{LW}, γ_S^-, γ_S^+) and surface tension parameters of deionized water (γ_W^{LW}, γ_W^-, γ_W^+) by using Eq. (5) (van Oss, 1995):

$$\Delta G(mJm^2) = -2(\gamma_S^{LW} - \gamma_W^{LW})^2 - 4(\sqrt{\gamma_S^+\gamma_S^-} + \sqrt{\gamma_W^+\gamma_W^-} - \sqrt{\gamma_S^+\gamma_W^-} - \sqrt{\gamma_S^-\gamma_W^+}) \quad (5)$$

2.4.5. Swelling capacity

The swelling behavior of the nonwovens was evaluated by using a gravimetric method. Thus, the nonwovens were cut into strips (2 cm × 2 cm), weighted and then immersed in 25 mL of phosphate-buffered saline (PBS), pH 7.4 at 37 °C in an incubator. At predetermined time up to 6 h, the samples were taken out of the fluid, blot dried and weighed. The swelling ratio was calculated according to Eq. (6). Four repeats of each nonwoven composition were evaluated.

$$\text{SwellingRatio}(\%) = \frac{W_{wet} - W_{dry}}{W_{dry}}x100 \quad (6)$$

where, W_{dry} and W_{wet} correspond to the weight of dried and swollen mats, respectively.

2.4.6. Water vapor transmission rate

The water vapor transmission rate (WVTR) was measured following a modified E96/E96 M −16 method (ASTME96/E96M-16, 2016). A circular nonwoven specimen (2.5 cm diameter) was mounted on the mouth of a glass bottle containing 20 mL deionized water. The bottles were weighed and placed in a controlled chamber set at 37 °C and maintained at controlled relative humidity (33%) for 24 h and weighed again. The WVTR ($g/m^2.24\ h$) was calculated as WVTR = (Δm)/(At), where Δm is the weight loss of each bottle, A is the nonwoven area exposed to the moisture transfer, and t is the time. Tests were replicated four times for each nonwoven composition.

2.4.7. In vitro enzymatic degradation

The *in vitro* biodegradability of nonwovens was studied by incubating them at 37 °C for 14 days in PBS containing lysozyme (5500 U/mL). Samples with dimensions of 1 cm × 1 cm were cut from nonwovens, weighed and placed into individual vials (20 mL) containing 5 mL of buffer solution. At predetermined incubation times (6 h, 12 h, 1, 2, 4, 7 and 14 days), samples were removed from the buffer, washed with deionized water, freeze-dried at −55 °C for 48 h, and weighed. The mass percent remaining of the nonwoven was calculated according to Eq. (7). Control tests, which correspond to incubation in absence of lysozyme, were also carried out. All experiments were carried out in triplicate.

$$\text{Massremaining}(\%) = \left(\frac{Wt}{W0}\right)x100 \quad (7)$$

where W_0 is the initial weight of the nonwoven and W_t is its weight after degradation.

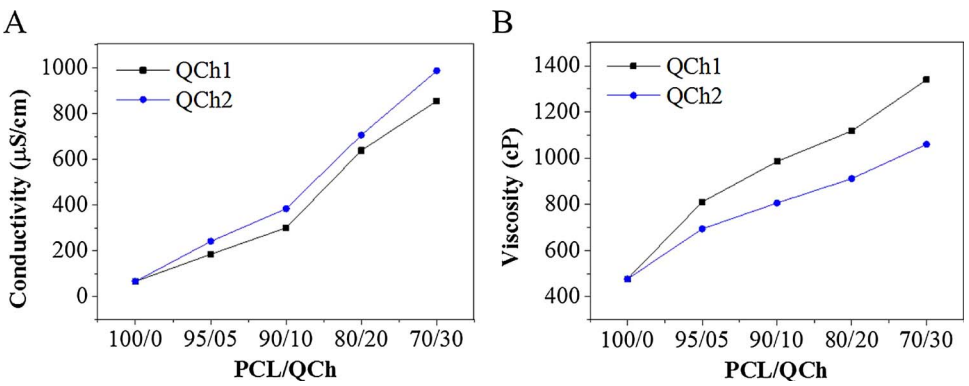

Fig. 1. Dependence of conductivity (A) and dynamic viscosity (B) of the spinning solutions as function of PCL/QCh weight ratio.

2.4.8. Tensile properties

Tensile tests of nonwovens were carried out on a Q800 from TA Instruments in tension mode using a thin film clamp under dry state and hydrated state, *i.e.* after swollen the nonwovens in PBS buffer (pH = 7.4) at 37 °C for 4 h, and in the perpendicular and parallel directions of the rotating drum collector (see Fig. S1, supplementary material). In all cases, rectangular specimens (20 mm × 6.4 mm) were cut from each nonwoven. The distance between grips was kept at 5 mm, and the tests were carried out with ramp strength of 1 N/min up to 18 N. The measurements were carried out at 25 °C. To carry out the mechanical tests in the hydrated state, the samples were taken out of the PBS, blot dried gently to remove excess fluid and immediately measured at 25 °C. At least five samples were tested for each type of specimen and the tensile strength (MPa), elastic modulus (MPa) and elongation-at-break (%) were determined from stress-strain curves.

2.4.9. Cytotoxicity assays

To determine the cytotoxicity of the nonwovens, HDFn cells were exposed to extracts of the nonwovens, which were produced according to the methodology adapted from ISO 10993-5 (ISO10993–5, 2009) and described by Neamnark et al. (2007). Briefly, PCL, PCL/QCh1 90/10, PCL/QCh2 90/10, PCL/QCh1 70/30 and PCL/Qch2 70/30 nonwovens strips (25 mm × 25 mm) were sterilized under UV light and extracts were prepared through 24 h incubation with fresh phenol-red free DMEM supplemented with 10% FBS at 37 °C and 5% CO_2 atmosphere (extraction ratio: 5 mg mL^{-1}). 96 well-plates were seeded with 5×10^4 cells/mL in DMEM supplemented with 10% FBS and incubated in humidified incubator at 37 °C and 5% of CO_2 for 24 h. Cell medium was then replaced by 100 μL of pure (5 mg/mL) or serial diluted nonwovens extracts (1, 0.5 and 0.25 mg/mL) or phenol-red free DMEM with 10% FBS (control group) and the plates were incubated for 24 h in humidified incubator. Cell viability was assessed indirectly by the MTT assay (5 mg/mL). Absorbance values were measured with the microplate spectrophotometer Multiskan™ GO (Thermo Fischer Scientific) at 570 nm, and viability values were calculated considering the absorbance values of the control group (cells that weren't exposed to nonwovens extracts) as 100% of viability. Experiments were conducted with triplicates of each group and repeated in three different occasions (total n = 9).

2.4.10. Cell adhesion

To evaluate cell adhesion and spreading, sterilized nonwovens strips (25 mm × 25 mm) were exposed to fresh culture medium in 6-well plates for 12 h at 37 °C and 5% of CO_2 before 2×10^5 HDFn cells were seeded onto the nonwovens (or onto the well's surface – control group) and incubated for additional 12 h in humidified incubator. Cells were fixated with 3.5% glutaraldehyde overnight and carefully washed three times with PBS (pH 7.4). Samples were dehydrated in ascending ethanol solution grades (30/50/70/80/90/100%), dried in HDMS and sputter coated with gold using the JFC-1600 coater. The cell morphology and attachment manner were evaluated *via* SEM analysis.

2.5. Statistical analysis

Experimental results were represented as the mean ± standard deviation. Statistical evaluation was carried out by analysis of variance (ANOVA) followed by multiple comparison tests using Tukey's test at the 95% confidence level. Statistical analyses were conducted using the open-source statistical programming language R v. 3.1.1.

3. Results and discussion

In this study, electrospun nonwovens of poly(caprolactone) and *N*-(2-hydroxy)-propyl-3-trimethylammonium chitosan chloride in weight ratios 100/0, 95/05, 90/10, 80/20 and 70/30 were prepared by using acetic acid-formic acid (60/40 v/v) as spinning solvent. Conditions of electrospinning were carefully investigated by carrying out a series of runs at different electric field strength, polymer concentration, and flow rate. Suitable conditions for electrospinning PCL and PCL/QCh blend solutions were 25 kV with a tip-to-collector distance of 15 cm and flow rate of 15 μL/min. Thus, results correspond to electrospun fiber nonwovens produced from solutions that were processed under the electrospinning conditions stated above and operating at 25 ± 2 °C and 60 ± 5% as the relative humidity.

It is well-known that the spinnability of polymer solutions and the morphology of electrospun fibers are affected by the solution properties, such as concentration, viscosity, conductivity, and surface tension. Although all these parameters are important, the solution viscosity and conductivity are the main parameters that affect the final characteristics of electrospun fibers (Bhardwaj & Kundu, 2010). The dependence of the solution conductivity as a function of the weight ratio PCL/QCh (Fig. 1A) reveals that it increases with increasing QCh concentration and the more substituted the chitosan derivative (QCh2/ $\overline{DQ}$ = 71.1 ± 0.8%; $\overline{DPv}$ = 1427), showing that the solution conductivity depends mainly on the total content of positive charges due to quaternized nitrogen atoms of QCh. The solution viscosity also increases with increasing QCh concentration (Fig. 1B) but such an effect is more pronounced in solutions containing the less substituted chitosan derivative (QCh1/$\overline{DQ}$ = 47.3 ± 0.4%; $\overline{DPv}$ = 2218). In this case, the higher viscosity average degree of polymerization of QCh1 is responsible for such a dependence of solution viscosity on the weight ratio PCL/QCh. The attempts to produce fiber nonwovens from spinning solutions containing more than 30% of QCh were unsuccessful as they resulted in solution spraying rather than jetting. Indeed, the electrospinning of such concentrated QCh solutions was precluded due to the strong repulsive forces among the positively charged substituent groups ($-N^+(CH3)_3$) and protonated amino groups of 2-amino-2-deoxy-D-glupyranose units pertaining to the parent chitosan, which can prevent the continuous formation of fibers according to the literature (Alipour et al., 2009).

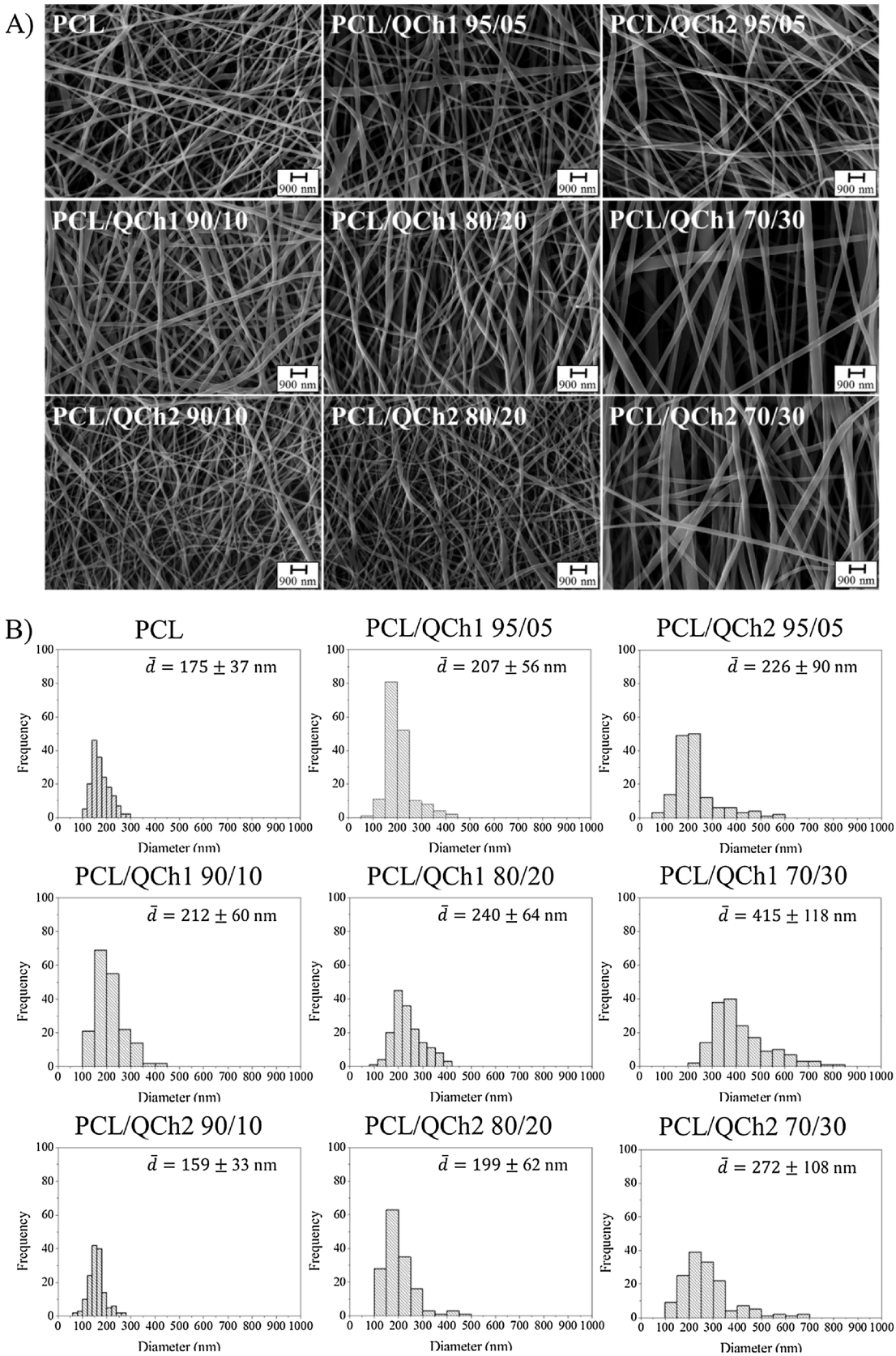

Fig. 2. SEM images of nonwovens PCL/QCh (A) and corresponding histograms showing fiber diameter distributions (B).

The electrospun fiber nonwovens produced from PCL solution and PCL/QCh blend solutions were cut into strips (8 mm × 6 mm) and then submitted to SEM analysis (Fig. 2A) in the direction perpendicular to the rotating drum collector (see Fig. S1 – Supplementary material). As seen in Fig. 2A, all solutions used to carry out the electrospinning experiments yielded defect-free, beadless, and geometrically uniform

Table 1
Average fiber diameter (nm), coherency coefficient and porosity (%) of PCL and PCL/QCh nonwovens.

Sample*	Fiber diameter (nm)	Coherency coefficient	Porosity (%)
PCL	175 ± 37[a]	0.31 ± 0.05[a]	58.5 ± 4.3[a]
PCL/QCh1 95/05	207 ± 55[b]	0.29 ± 0.03[a]	57.0 ± 1.6[a]
PCL/QCh2 95/05	226 ± 90[b,c]	0.32 ± 0.02[a]	61.4 ± 2.8[a]
PCL/QCh1 90/10	212 ± 61[b]	0.27 ± 0.01[a]	70.5 ± 2.1[b,d]
PCL/QCh2 90/10	159 ± 33[a]	0.22 ± 0.01[b]	81.6 ± 2.0[c]
PCL/QCh1 80/20	240 ± 62[c]	0.39 ± 0.02[c]	74.3 ± 1.4[b,c]
PCL/QCh2 80/20	199 ± 62[a,b]	0.22 ± 0.01[b]	71.3 ± 1.0[b,d]
PCL/QCh1 70/30	415 ± 117[d]	0.52 ± 0.04[d]	61.5 ± 4.0[a,d]
PCL/QCh2 70/30	272 ± 108[e]	0.43 ± 0.01[c]	66.0 ± 2.4[b,d]

* Means followed by the same letter do not differ by Tukey test at 5% probability.

fibers. However, the corresponding fiber diameter histograms (Fig. 2B) reveal that the fiber average diameters were noticeably affected by the composition of the spinning solutions. In most PCL/QCh nonwovens the fibers displayed diameters predominantly in the range 100 nm–350 nm but high contents of QCh resulted in higher fiber diameter and broader distribution. Accordingly, the fiber average diameter of the PCL nonwoven was significantly lower (175 ± 37 nm) as compared to PCL/QCh1 70/30 (415 ± 118 nm). Comparing the nonwovens containing QCh1 and QCh2 reveals that thinner fibers were formed when the latter chitosan derivative was present in the polymer blend, which may be related to the higher conductivity and lower viscosity of the blend solutions PCL/QCh2. In contrast, the electrospinning of solutions displaying high viscosity and conductivity gave rise to thicker fibers and broader fiber diameter distribution. Such a behavior can be attributed to the high viscosity of the spinning solution, which leads to the ejection of thicker jets, and to its high conductivity, which increases the instability of the ejected jets, thus increasing the broadness of fiber diameter distribution (Bhardwaj & Kundu, 2010).

According to the coherency coefficients of fibers (Table 1), PCL/QCh1 80/20, PCL/QCh1 70/30 and PCL/QCh2 70/30 nonwovens exhibited a predominant fiber orientation pattern, which was evaluated by using a color-coded map (Fig. S2, supplementary material), revealing a predominant orientation angle ≈ 90°. This behavior is attributed to the higher viscosity of the blend solutions which were electrospun to produce these nonwovens. Thus, as the fiber collects onto the collector surface, it is attached to it and stretchs the following tow of fiber from its spiraling path to align with the rotation direction of the collector. When high viscosity polymer solutions are electrospun, the effective draw is increased due to the decrease of fractures of the ejected jets, resulting in better matching between the fiber orientation deposition and the rotation direction of the collector, improving the alignment of the collected fibers (Bhardwaj & Kundu, 2010; Fennessey & Farris, 2004).

A possible application of PCL/QCh nonwovens presenting random and highly aligned fibers is in Tissue Engineering and Regenerative Medicine as such characteristics may improve the adhesion, spreading and proliferation of cells. Additionally, the high porosity of the nonwovens (Table 1), which ranged in a relatively narrow interval (57.0 ± 1.6% − 81.6 ± 2.0%), is an interesting characteristic concerning its potential use as a wound dressing since it could contribute to improve the gas exchange, to facilitate the transfer of nutrients to the cells as well as the absorption of exudate, thus favoring the wound healing (Liang et al., 2016).

3.1. Fourier transform infrared spectroscopy

ATR-FTIR analysis was carried out to characterize the presence of functional groups in the surface of QCh, PCL/QCh and PCL nonwovens (Fig. 3). The IR spectrum of QCh2 (powder form) is characterized by absorption bands at: *i*) 3349 cm^{-1} due to the stretching vibration of OH and NH_2 groups; *ii*) 2943 and 2865 cm^{-1} attributed to C−H stretching vibrations; *iii*) 1653 cm^{-1} due to C=O stretching of amide I; *iv*) 1572 cm^{-1} due to N−H bending of primary amine; *v*) 1472 cm^{-1} due to C−H bending of $-^{+}N(CH_3)_3$ groups; *vi*) 1157–1030 cm^{-1} attributed to the stretching of C−O of 2-amino-2-deoxy-D-glupyranose units (Santos et al., 2016). The spectrum of PCL nonwoven exhibits distinctive bands at 2948 and 2868 cm^{-1} attributed to C−H stretching vibrations and an intense and sharp band at 1726 cm^{-1} that correspond to the carbonyl stretching of a carboxylic ester. The bands in the range of 1157 − 1030 cm^{-1} correspond to C−O−C stretching vibrations and the band at 1385 cm^{-1} is related to the H−C−O in-plane bending (Diez-Pascual & Diez-Vicente, 2016). The spectrum of the PCL/QCh2 70/30 nonwoven shows the characteristic bands of both QCh and PCL. Absorption bands at 3349 and 1572 cm^{-1} are ascribed to the O−H and N−H stretching and N−H bending of QCh, respectively, whereas the band at 1730 cm^{-1} correspond to the C=O stretching of PCL. Similar bands were also observed in the spectra of the other PCL/QCh nonwovens. Comparing the spectra of PCL/QCh2 nonwovens in the range 3000 − 3600 cm^{-1} (Fig. 3B) clearly shows that the intensity of the band centered at 3349 cm^{-1} gradually increased with increasing QCh content, which is attributed to the increase of $-NH_2$ and −OH groups on the surface of nonwovens. A similar trend was also observed in the spectra of PCL/QCh1 nonwovens.

3.2. Surface free energy and hydrophilicity of nonwovens

Aiming to evaluate the hydrophilicity of the surface of PCL/QCh nonwovens, the average contact angle (CA) was measured as a function of the probe liquid (Table S1, Supplementary Information). From the values of CA and by using the approach proposed by Good, van Oss and Chaudhery (acid–base theory), the surface energy components, namely dispersive (γ^{LW}), acid-base (γ^{AB}), electron-donor (γ^{-}) and electron-acceptor (γ^{+}) components, were calculated (Table 2). The dispersive component (γ^{LW}) comprises the capacity of the molecules at the probed surface to take part in van der Waals interactions while the acid-base component (γ^{AB}), also called polar component, accounts for all the other possible interactions (induction, dipole, and hydrogen bond), being composed by electron-donor (γ^{-}) and electron-acceptor (γ^{+}) parameters ($\gamma^{AB} = 2\sqrt{\gamma^{-}\gamma^{+}}$) (van Oss, 1995).

The data in Table 2 show that the contribution of the dispersive component to the total surface free energy of the nonwovens is larger than the contribution of the polar component, but this latter becomes more important the higher the QCh content. Thus, comparing the PCL and PCL/QCh2 70/30 nonwovens reveals that the polar component contribution represents 3% and 15%, respectively, of their total surface energy. Additionally, the comparison of the same two nonwovens reveals that the QCh content strongly affects the electron-donor component (γ^{-}), which increases from 1.0 ± 0.3 mJ m^{-2} (PCL nonwoven) to 47.8 ± 1.4 mJ m^{-2} (PCL/QCh2 70/30 nonwoven). Indeed, the average degree of quaternization of QCh also affects the electron-donor component (γ^{-}) as PCL/QCh2 nonwovens present higher values of γ^{-} as compared to PCL/QCh1 nonwovens ($p < 0.05$), except when the QCh content is below 10%. Also, as long as the QCh content is equal or higher than 10%, the surfaces of the nonwovens present predominantly monopolar electron-donicity ($\gamma^{-} \gg \gamma^{+} \approx 0$), revealing their electron donating capacity and ability to participate in polar interactions with acid species (van Oss, 1995).

The surface energy components of the PCL/QCh nonwovens were used to calculate ΔG (Table 2), the interfacial free energy of interaction, which may be used as a quantitative measure of surface hydrophilicity or hydrophobicity. As by convention $\Delta G > 0$ characterizes the surface of a given material as hydrophilic while hydrophobic surfaces are characterized by $\Delta G < 0$, the data in Table 2 reveals that the values of interfacial free energy of interaction become less negative with increasing QCh content and the higher the average degree of substitution of QCh, which corroborates the evidences that more hydrophilic groups

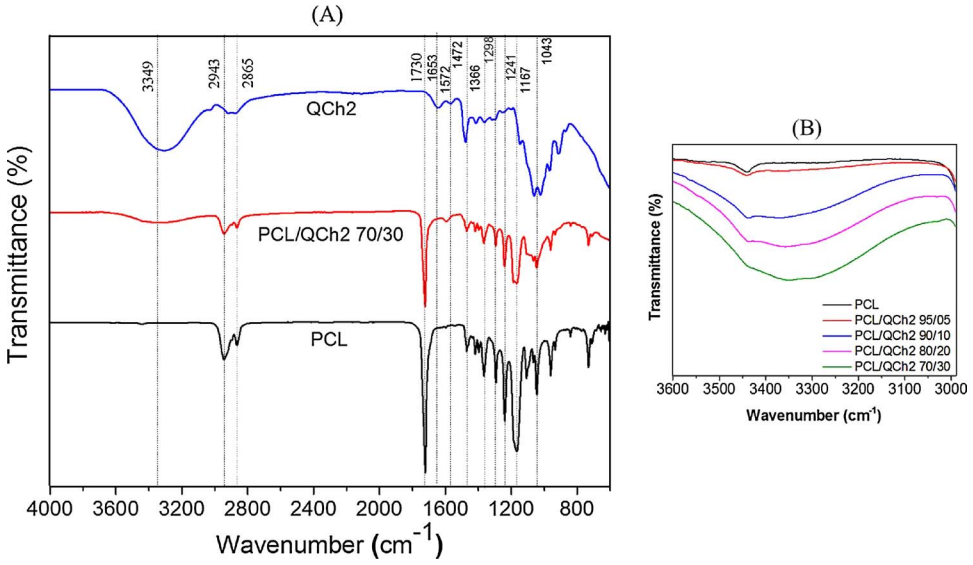

Fig. 3. ATR-FTIR spectra of QCh2 (powder form), PCL/QCh2 70/30 and PCL nonwovens (A); IR spectra in the range 3000–3600 cm^{-1} showing the comparison between PCL/QCh2 formulations (B).

are exposed at the surface of the PCL/QCh nonwovens the higher the QCh content. In fact, the results expressed in Table 2 corroborate the findings from ATR-FTIR spectroscopy, which evidenced the presence of hydrophilic groups, mainly OH and NH_2 groups, in the surface of PCL/QCh nonwovens.

According to some authors, materials surfaces exhibiting moderate hydrophilicity, *i. e.* the contact angle with water ranges as 40°–80°, favor the adhesion and proliferation of different cell types (Arima & Iwata, 2007; Harnett, Alderman, & Wood, 2007). Therefore, the results of this study show that all PCL/QCh nonwovens, except PCL/QCh 95/05 nonwoven, may favor the cellular activity and, consequently, improve the healing process.

3.3. Swelling capacity

The swelling capacity is an essential property of nonwovens aimed to be used as wound dressings, and knowing it allows one to estimate the role the nonwoven will play concerning the exudate management, and then the control of moisture balance at the wound surface (Ninan, Forget, Shastri, Voelcker, & Blencowe, 2016; Yoo & Kim, 2008). The measurements carried out to evaluate the swelling capacity of the nonwovens on PBS at 37 °C showed that it is strongly dependent on the nonwoven composition (Fig. 4A). Thus, the swelling equilibrium condition was reached after 120 min in the case of the PCL nonwoven but only 30 min were needed to attain it in the case of PCL/QCh nonwovens, regardless of the QCh content and its average degree of quaternization. However, the maximum swelling capacity increased with increasing QCh content and the higher the average degree of quaternization of QCh, which is attributed to the progressive increase of the hydrophilic character of nonwovens. Thus, for instance, the maximum swelling capacity of PCL/QCh2 70/30 nonwoven is at least twice that exhibited by PCL nonwoven. Additionally, porosity may also affect the swelling capacity of the nonwoven as a low porosity may restrict the free space available for water uptake. Accordingly, those nonwovens exhibiting low porosity, namely PCL and PCL/QCh 95/05 nonwovens, also displayed low swelling capacity. Results showed that the swelling capacity of PCL/QCh nonwovens can be controlled by selecting the QCh derivative in terms of average degree of quaternization and by adjusting the QCh content, allowing the development of dressings suitable to be applied to humid or dry wounds according to their swelling capacity. Indeed, owing to the high water absorption capacity of the nonwovens with QCh content ≥10%, these would be indicated for protection of highly exuding wounds.

3.4. Water vapor transmission rate (WVTR)

The ability of dressings to control the water loss from the wound to the atmosphere over a defined time is evaluated by determining their water vapor transmission rate (WVTR). Indeed, it is a very important dressing property as a high WVTR may lead to wound dehydration whereas a low WVTR may cause the accumulation of wound exudates and, consequently, raises the risk of contamination. In this sense, a dressing with a suitable WVTR is required to avoid excessive dehydration and exudate accumulation (Xu et al., 2016). The WVTR data of the PCL/QCh nonwovens are shown in Fig. 4B, revealing that it ranged in the interval 1600 $g/m^2.24\,h$–2500 $g/m^2.24\,h$ and according to the nonwoven composition. Thus, PCL/QCh1 70/30 nonwoven exhibited a very high WVTR (2435 ± 56 $g/m^2.24\,h$) while PCL and PCL/QCh 95/

Table 2
Calculated surface energy components* and interfacial free energy of interaction (ΔG) of nonwovens (in mJ m^{-2}).

Sample**	γ^{LW}	γ^-	γ^+	γ^{AB}	γ^{TOTAL}	ΔG
PCL	47.5 ± 0.1^a	1.0 ± 0.3^a	0.50 ± 0.01^a	1.4 ± 0.2^a	49.0 ± 0.4^a	-80.3 ± 2.8^a
PCL/QCh1 95/05	46.3 ± 0.3^a	0.9 ± 0.1^a	1.2 ± 0.1^b	2.1 ± 0.1^b	48.2 ± 0.1^a	-73.7 ± 1.3^b
PCL/QCh2 95/05	46.4 ± 0.2^a	0.9 ± 0.2^a	1.6 ± 0.1^c	2.3 ± 0.1^b	48.6 ± 0.3^a	-71.5 ± 0.3^b
PCL/QCh1 90/10	45.6 ± 0.5^{a,b}	16.1 ± 0.3^b	0.21 ± 0.01^d	3.7 ± 0.1^c	49.5 ± 0.4^a	-27.9 ± 1.0^c
PCL/QCh2 90/10	44.4 ± 0.7^b	19.5 ± 0.4^c	0.18 ± 0.03^d	3.7 ± 0.2^c	48.0 ± 0.7^a	-20.6 ± 0.2^d
PCL/QCh1 80/20	43.5 ± 0.7^b	17.7 ± 1.5^{c,b}	0.4 ± 0.05^f	5.2 ± 0.1^d	48.7 ± 0.8^a	-20.5 ± 1.6^d
PCL/QCh2 80/20	42.9 ± 0.4^{b,c}	24.3 ± 0.5^d	0.3 ± 0.01^g	5.5 ± 0.03^d	48.4 ± 0.7^a	-9.2 ± 0.5^e
PCL/QCh1 70/30	41.0 ± 1.2^c	37.7 ± 2.3^e	0.20 ± 0.02^d	5.1 ± 0.3^d	46.0 ± 0.4^b	+16.2 ± 2.7^f
PCL/QCh2 70/30	38.6 ± 1.3^d	47.8 ± 1.4^f	0.26 ± 0.03^g	7.0 ± 0.3^e	45.0 ± 0.6^b	+29.5 ± 2.1^g

* Dispersive (γ^{LW}), electron-donor (γ^-), electron-acceptor (γ^+), acid-base (γ^{AB}); total surface energy (γ^{TOTAL}).
** Means followed by the same letter in the columns do not differ by a Tukey's test at 5% probability.

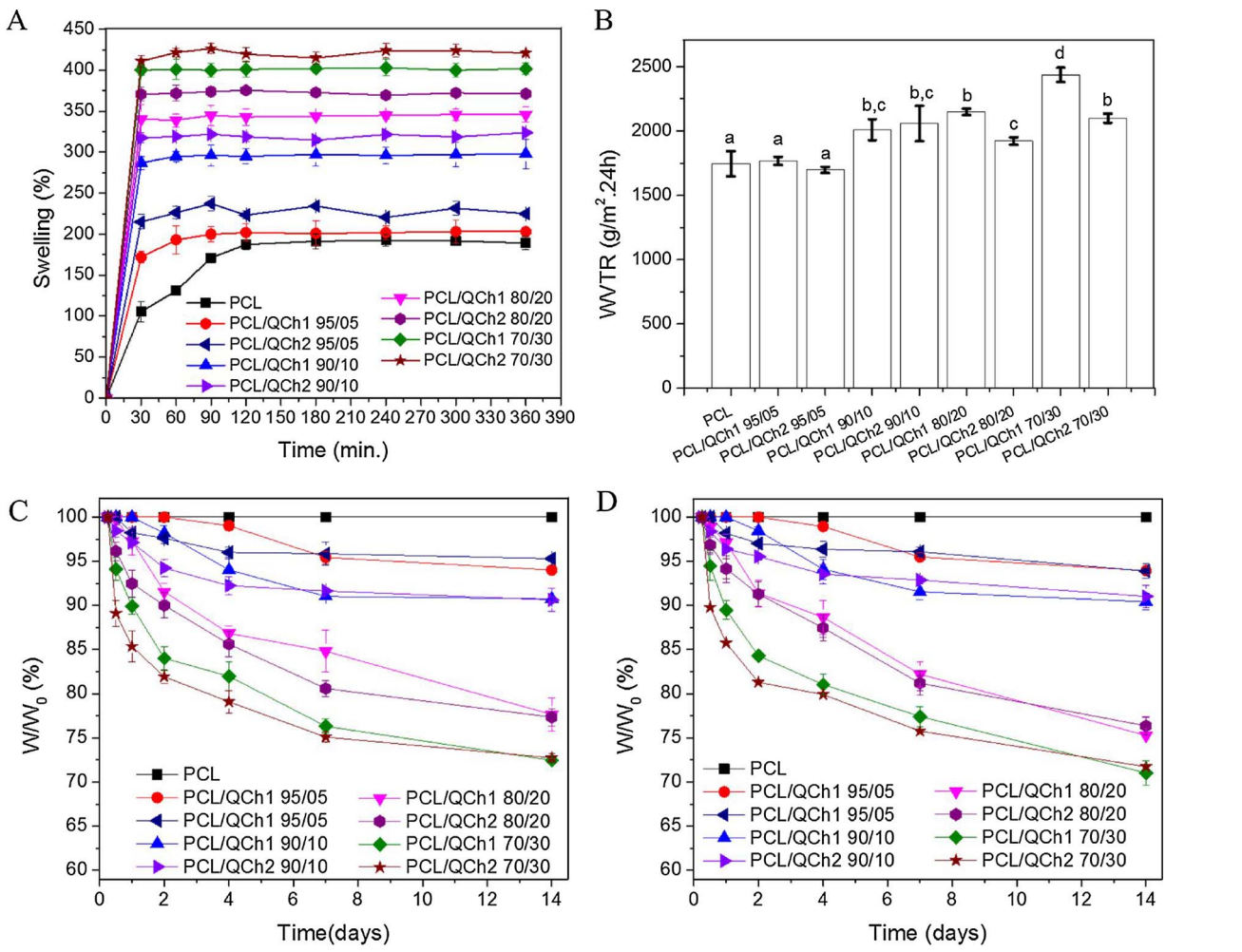

Fig. 4. - Swelling ratio (A) and water vapor transmission rate (WVTR) of nonwovens (B); in vitro degradation profiles of nonwovens in the presence (C) and absence (D) of lysozyme in a phosphate buffer solution (pH 7.4) at 37 °C.

05 nonwovens displayed much lower values of WVTR. The main factors affecting WVTR include the dressing porosity and hydrophilicity, the lower the former parameter the less important the barrier against water vapor transport while increasing the hydrophilicity favors the interactions involving water vapor molecules and the nonwoven, facilitating its transport across the nonwoven (Findenig et al., 2012). Thus, PCL and PCL/QCh 95/05 nonwovens, which exhibited low porosity and hydrophilicity, also displayed low WVTR values. As some studies have proposed that dressings exhibiting high WVTR (2000 g/m^2.24 h–2500 g/m^2.24 h) are able to maintain an adequate moisture at the wound surface(Chen, Yan, Yuan, Zhang, & Fan, 2011; Xu et al., 2016), all the PCL/QCh nonwovens of this study, except PCL/QCh 95/05 nonwovens, show potential to be used as dressings.

3.5. *In vitro* biodegradability

The *in vitro* enzymatic degradation study was carried out to evaluate the stability of nonwovens at the wound site concerning the possible action of lysozyme. Indeed, lysozyme is an important defense enzyme that acts by hydrolyzing the β (1 → 4) glycosidic bond between *N*-acetylmuramate and *N*-acetylglucosamine units present in the cell wall of Gram-positive bacteria (Niyonsaba & Ogawa, 2005). This enzyme is also present at the wound exudate in concentrations ranging between 1000 units/mL and 5500 units/mL and it is associated with the inflammatory response of the wound healing process (Buchan et al., 1981; Niyonsaba & Ogawa, 2005). Comparing the curves in Fig. 4C and D, which correspond to the *in vitro* degradation profiles of nonwovens in presence and absence of lysozyme (5500 units/mL), respectively, reveals that the weight loss with increasing incubation time is due to the dissolution of QCh in PBS rather than to the action of lysozyme. The lack of lysozyme activity may be attributed to: *i*) the low average degree of acetylation ($\overline{DA}$ = 7%) of the QCh derivatives (Santos et al., 2016), as the activity of lysozyme on chitosan-like substrates depends on the occurrence of sequences of diads *N*-acetilglucosamine/*N*-acetilglucosamine: *ii*) the presence of numerous positively charged sites on these polymer chains, which may precludes the fitness of the substrate to the active site; *iii*) polycaprolactone is not a substrate of lysozyme (Verheul et al., 2009; Woodruff & Hutmacher, 2010).

Thus, as expected, the PCL nonwoven did not degrade after 14 days, in the presence as well as in the absence of lysozyme, as it is not degraded by lysozyme neither dissolved by PBS. However, the loss of weight was more important the higher the QCh content and the higher its average degree of quaternization. Thus, after 14 days of incubation, substantially higher weight loss was observed for PCL/QCh 70/30 nonwovens (remaining weight ≈ 72%) as compared to PCL/QCh 95/05 nonwovens (remaining weight ≈ 94%). Such results indicate that the degradation rate of PCL/QCh nonwovens may be controlled by the selection of QCh derivative and by adjusting the nonwoven composition to meet the biodegradability requirements of the dressing according to the application. Additionally, the slow release of QCh from the PCL/QCh nonwovens may contribute to keep the wound site free of bacterial infection owing to the antimicrobial activity of QCh (Verlee, Mincke, & Stevens, 2017).

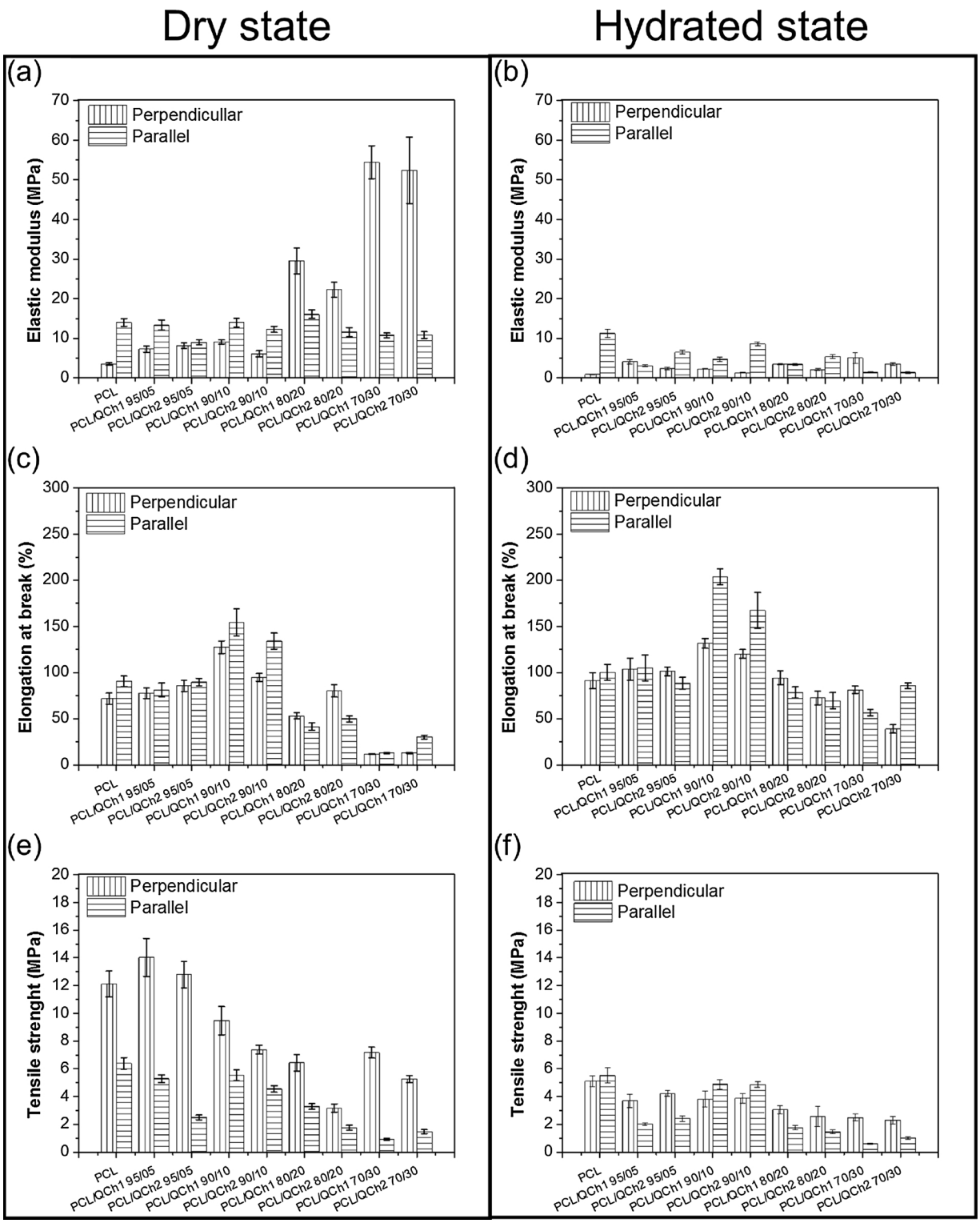

Fig. 5. Tensile properties of nonwovens (a,c and e) at dry state and (b,d and f) hydrated state.

3.6. Mechanical properties

Concerning practical aspects related to the wound dressing application, electrospun nonwovens should have reasonable mechanical properties to facilitate handling and application, and they must also provide and retain sufficient mechanical support for cell growth and proliferation during tissue regeneration (Gharibi, Yeganeh, Gholami, & Hassan, 2014; Gharibi, Yeganeh, Rezapour-Lactoee, & Hassan, 2015). Therefore, the mechanical properties of PCL/QCh nonwovens were evaluated by carrying out tensile tests in the perpendicular and parallel directions under dry and hydrated states. The elastic modulus, tensile strength, and elongation-at-break of the PCL/QCh nonwovens are presented in Fig. 5.

Under dry state, the higher elastic moduli, taken in the perpendicular direction of the collector, were observed in the cases of nonwovens richer in QCh, namely the nonwovens PCL/QCh1 70/30 and PCL/QCh2 70/30, which values were 54.4 ± 4.1 MPa and 52.4 ± 8.4 MPa, respectively. However, these nonwovens exhibited

low elongation-at-break in both directions, whereas the nonwovens PCL/QCh1 90/10 and PCL/QCh2 90/10 showed higher elongation in the perpendicular (127.4 ± 6.9% and 94.9 ± 4.3%, respectively) and parallel directions (154.4 ± 14.9% and 134.2 ± 8.8%, respectively). The lowest tensile strength was observed in nonwovens presenting high QCh content. Such mechanical behavior may be attributed to the high interfacial interaction of PCL and QCh at higher QCh content, which limits the mobility of PCL chains resulting in poor mechanical properties (Khan et al., 2013). It is interesting to note that the highest tensile strength was observed in the perpendicular direction for all nonwovens and, considering the same PCL/QCh weight ratio, the nonwovens containing QCh1 showed higher tensile strength as compared to QCh2 in at least one of the directions of analysis. The high tensile strength in the perpendicular direction for all nonwovens can be explained by the presence of aligned fibers on the samples, as observed in SEM images (Fig. 2A). On the other hand, the lower degree of polymerization of QCh2 as compared to QCh1 favors the interfacial interaction of PCL and QCh that results in loss of mobility of PCL chains, restraining stress movement and, consequently, decreasing the tensile strength (Hejna, Formela, & Saeb, 2015).

Tensile tests were also carried out on fully hydrated nonwovens to evaluate their applicability for the protection of high exuding wounds. Fig. 5b, d and f shows that the mechanical properties of the nonwovens changed upon exposure to PBS solution. Then, all nonwovens exhibited lower elastic modulus and tensile strength, whereas an expressive increase of elongation-at-break was observed at least in one tested direction. This mechanical behavior is attributed to the plasticizing effect of the absorbed water molecules, which increases the elasticity and elongation of the nonwovens while reduces its strength (Gharibi et al., 2014). Nonwovens with high QCh content (PCL/QCh1 70/30, PCL/QCh2 70/30) showed high increase of elongation-at-break in both directions under hydrated state as consequence of their superior water absorption capacity. On the contrary, as consequence of the deterioration of intermolecular interactions involving polymer chain segments due to presence of water molecules, these nonwovens showed lower tensile strength as compared to the other nonwovens.

The mechanical properties of human skin depend on age, sex and body region, the elastic modulus ranging between 0.4 and 20 MPa, elongation between 10% and 115%, and tensile strength between 2.5 and 30 MPa (Edwards & Marks, 1995; Jussila, Leppäniemi, Paronen, & Kulomäki, 2005; Pailler-Mattei, Bec, & Zahouani, 2008; Sugihara, Ohura, Homma, & Igawa, 1991). It is worth mentioning that the comparison of tensile properties of human skin described in literature and the values obtained in this study should be taken with prudence since a direct comparison is not entirely valuable due the differences in the conditions the mechanical tests were carried out. However, the tensile properties and elongation-at-break of the PCL/QCh nonwovens indicate that most of them can be considered as potential materials for wound dressings. Also, PCL/QCh1 90/10 and PCL/QCh2 90/10 nonwovens seem to be the best candidates for such an application as they presented high tensile strength and elongation under dry and hydrated states.

3.7. Cytotoxicity and cell adhesion

The study on the *in vitro* cell viability is important to evaluate the biocompatibility of the materials and it is required to develop the *in vivo* studies and for clinical use. Fibroblasts, the most common cells of the connective tissue, play an essential role in wound healing process, creating new extra cellular matrix (ECM) and collagen structures to support the other cells related to an effective wound healing, as well as contracting the wound (Kalluri & Zeisberg, 2006; Werner, Krieg, & Smola, 2007). In this sense, aiming to evaluate the cytotoxic effect of nonwovens, neonatal human dermal fibroblast (HDFn) cells were exposed to varying extraction ratios of the PCL, PCL/QCh1 90/10, PCL/QCh2 90/10, PCL/QCh1 70/30 and PCL/QCh2 70/30 nonwovens (0.25–5 mg/mL) for 24 h and then submitted to the MTT viability assay (Fig. 6a).

According to ISO 10993-5(ISO10993–5, 2009), a reduction of cell viability to less than 70% is taken as evidence of a cytotoxic effect. Thus, PCL, PCL/QCh1 90/10, PCL/QCh2 90/10, PCL/QCh1 70/30 nonwovens are not cytotoxic as the percentages of viable cells remains above 70%, regardless of the extraction ratio (Fig. 6). On the other hand, PCL/QCh2 70/30 nonwoven presents significant toxicity to the cells even at low extraction ratio (0.25 mg/mL), and it severely affects cell viability when extraction ratio surpass 1 mg/mL. Considering that the cell viability analyses were carried out with the extracts prepared through the exposition of nonwovens to incubation medium and that PCL is biocompatible and insoluble in aqueous solutions, the slight decrease of cell viability provoked by most of the PCL/QCh nonwovens can be attributed to the presence of the quaternized chitosan derivative in the incubation medium. In fact, results show that the cell viability decreases with increasing QCh content in the PCL/QCh nonwovens and with increasing degree of quaternization of QCh, supporting the assumption that QCh is partially dissolved in the incubation medium. Additionally, the higher average number of cationic groups per repeating unit of QCh2 as compared to QCh1 results in a more pronounced cytotoxic effect, the higher charge density of QCh2 chains favoring the establishment of strong electrostatic interactions with the negatively charged sites on the fibroblast membrane, which can result in cell membrane damage (Fischer, Li, Ahlemeyer, Krieglstein, & Kissel, 2003; Wongwanakul et al., 2017).

The establishment of interactions between the biomaterial and cells is considered the vital step toward tissue regeneration, so this phenomenon was evaluated via SEM (Fig. 6b). Few or no cells were able to effectively attach to the surface of the PCL nonwoven, while PCL/QCh1 90/10, PCL/QCh2 90/10 and PCL/QCh1 70/30 nonwovens showed the spreading of cellular mass throughout their surfaces with extended pseudopodia-like structure. HDFn cells assumed a more spindle-shaped morphology and they oriented parallel to the nanofibers in the surface PCL/QCh1 70/30 nonwoven, that one which presented the higher coherency coefficient (Table 1). However, low cell adhesion was observed in the surface of PCL/QCh2 70/30 nonwoven, a result well correlated to the cytotoxic profile observed when cells were exposed to extracts of this nonwoven. Furthermore, some cells attached to the surface of the PCL/QCh2 70/30 nonwoven displayed a rough topology that might indicate an early stage of apoptosis induced by the nonwoven. These results suggest that the PCL/QCh nonwovens had improved cell adhesion and proliferation compared to the PCL nonwoven, which may be attributed to the higher hydrophilicity of the surface of the formers as compared to the latter (Arima & Iwata, 2007; Harnett et al., 2007). However, materials surfaces exhibiting moderate hydrophilicity (*i.e.* PCL/QCh1 90/10 and PCL/QCh2 90/10) were more favorable for adhesion and proliferation of fibroblasts. Thus, although further in vivo investigations are required to fully validate the PCL/QCh1 90/10, PCL/QCh2 90/10 and PCL/QCh1 70/30 nonwovens, it can be concluded that they are potential candidates for wound healing and tissue engineering applications.

4. Conclusion

The morphology and properties of the electrospun nonwovens composed by poly(ε-caprolactone) (PCL) and *N*-(2-hydroxy)-propyl-3-trimethylammonium chitosan chloride (QCh) strongly depend on the content of the quaternized chitosan derivative, on its average degree of quaternization ($\overline{DQ}$) and viscosity average degree of polymerization ($\overline{DPv}$), as well as on the alignment of the nanofibers conferred by using a drum rotating collector during the electrospinning process. Thus, the nanofibers average diameter and the nonwovens porosity can be controlled by properly selecting the QCh derivative and its content on the resulting PCL/QCh nonwoven. The surface of PCL nonwoven is hydrophobic, as showed by FTIR-ATR spectroscopy and contact angle measurements, but as the QCh content in the PCL/QCh nonwovens

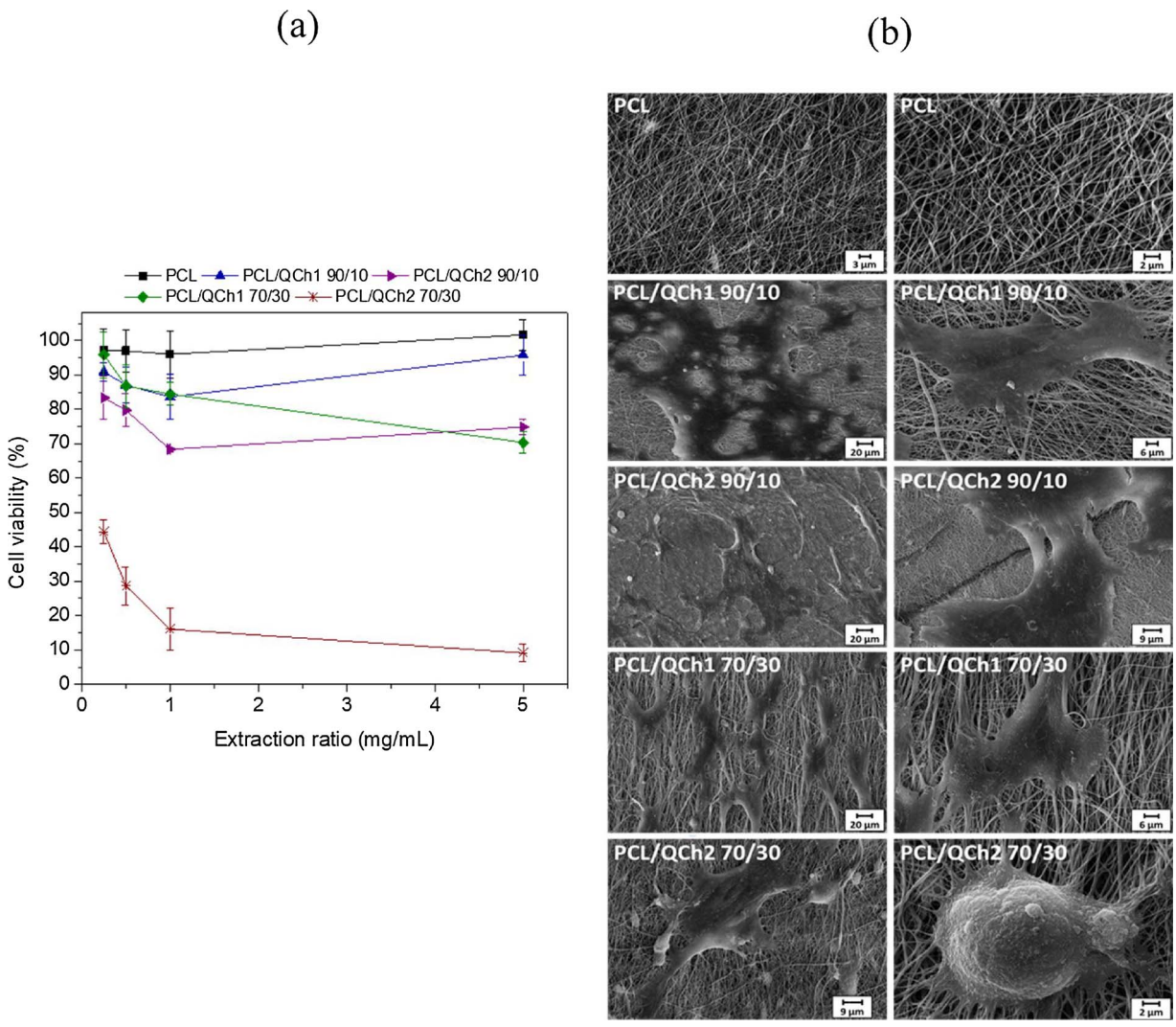

Fig. 6. (a) dependence of the HDFn cell viability on the nonwovenścomposition and extraction ratios. The viability of the control cell was set at 100%, and viability relative to control was expressed; (b) SEM images of HDFn cells cultured onto PCL, PCL/QCh1 90/10, PCL/QCh2 90/10, PCL/QCh1 70/30 nonwovens for 12 h.

increases the surface hydrophilicity is increased, strongly favoring HDFn cells' adhesion and spreading. Moreover, the improved nanofibers alignment observed in PCL/QCh1 70/30 nonwoven favored the relative orientation of HDFn cells indicating possible applications in Tissue Engineering and Regenerative Medicine. All PCL/QCh nonwovens were non-cytotoxic, except PCL/QCh2 70/30 nonwoven that exhibited severe cytotoxicity, which is attributed to the partial release of QCh2 to the culture medium. The physicochemical and mechanical properties of PCL/QCh nonwovens indicate the potential of these materials as wound dressings. Taking into account the whole set of results, it is concluded that the electrospun nonwovens composed by poly(ε-caprolactone) (PCL) and *N*-(2-hydroxy)-propyl-3-trimethylammonium chitosan chloride (QCh) are nanofibers-based biomaterials potentially useful as wound dressings, mainly the nonwovens PCL/QCh 90/10 that strongly favored the adhesion and spreading of HDFn cells.

Acknowledgments

The authors are grateful to Coordenação de Aperfeiçoamento de Pessoal de Nível Superior (CAPES 443/2012; Brazil), Conselho Nacional de Desenvolvimento Científico e Tecnológico (CNPq 142002/2014-3; CNPq 311250/2016-5; Brazil) and Fundação de Amparo à Pesquisa do Estado de São Paulo (FAPESP 2010/02526-1; Brazil) for financial support.

Appendix A. Supplementary data

Supplementary data associated with this article can be found, in the online version, at https://doi.org/10.1016/j.carbpol.2018.01.045.

References

ASTME96/E96M-16 (2016). *Standard test methods for water vapor transmission of materials.* West Conshohocken, PA: ASTM Internationalhttp://dx.doi.org/10.1520/E0096_E0096M-16.

Abrigo, M., McArthur, S. L., & Kingshott, P. (2014). Electrospun nanofibers as dressings for chronic wound care: Advances, challenges, and future prospects. *Macromolecular Bioscience, 14*(6), 772–792. http://dx.doi.org/10.1002/mabi.201300561.

Alipour, S. M., Nouri, M., Mokhtari, J., & Bahrami, S. H. (2009). Electrospinning of poly (vinyl alcohol)–water-soluble quaternized chitosan derivative blend. *Carbohydrate Research, 344*(18), 2496–2501. http://dx.doi.org/10.1016/j.carres.2009.10.004.

Arima, Y., & Iwata, H. (2007). Effect of wettability and surface functional groups on protein adsorption and cell adhesion using well-defined mixed self-assembled monolayers. *Biomaterials, 28*(20), 3074–3082. http://dx.doi.org/10.1016/j.biomaterials.2007.03.013.

Bhardwaj, N., & Kundu, S. C. (2010). Electrospinning: A fascinating fiber fabrication technique. *Biotechnology Advances, 28*(3), 325–347. http://dx.doi.org/10.1016/j.biotechadv.2010.01.004.

Boateng, J. S., Matthews, K. H., Stevens, H. N. E., & Eccleston, G. M. (2008). Wound healing dressings and drug delivery systems: A review. *Journal of Pharmaceutical Sciences, 97*(8), 2892–2923. http://dx.doi.org/10.1002/jps.21210.

Buchan, I. A., Andrews, J. K., Lang, S. M., Boorman, J. G., Harvey Kemble, J. V., & Lamberty, B. G. H. (1981). Clinical and laboratory investigation of the composition and properties of human skin wound exudate under semi-permeable dressings. *Burns,*

7(5), 326–334. http://dx.doi.org/10.1016/0305-4179(81)90005-X.
Chen, Y., Yan, L., Yuan, T., Zhang, Q., & Fan, H. (2011). Asymmetric polyurethane membrane with in situ-generated nano-TiO2 as wound dressing. *Journal of Applied Polymer Science, 119*(3), 1532–1541. http://dx.doi.org/10.1002/app.32813.
Cipitria, A., Skelton, A., Dargaville, T. R., Dalton, P. D., & Hutmacher, D. W. (2011). Design, fabrication and characterization of PCL electrospun scaffolds-a review. *Journal of Materials Chemistry, 21*(26), 9419–9453. http://dx.doi.org/10.1039/C0JM04502K.
Diez-Pascual, A. M., & Diez-Vicente, A. L. (2016). Electrospun fibers of chitosan-grafted polycaprolactone/poly(3-hydroxybutyrate-co-3-hydroxyhexanoate) blends. *Journal of Materials Chemistry B, 4*(4), 600–612. http://dx.doi.org/10.1039/C5TB01861G.
Edwards, C., & Marks, R. (1995). Bioengineering of the SkinEvaluation of biomechanical properties of human skin. *Clinics in Dermatology, 13*(4), 375–380. http://dx.doi.org/10.1016/0738-081X(95)00078-T.
Fennessey, S. F., & Farris, R. J. (2004). Fabrication of aligned and molecularly oriented electrospun polyacrylonitrile nanofibers and the mechanical behavior of their twisted yarns. *Polymer, 45*(12), 4217–4225. http://dx.doi.org/10.1016/j.polymer.2004.04.001.
Findenig, G., Leimgruber, S., Kargl, R., Spirk, S., Stana-Kleinschek, K., & Ribitsch, V. (2012). Creating water vapor barrier coatings from hydrophilic components. *ACS Applied Materials & Interfaces, 4*(6), 3199–3206. http://dx.doi.org/10.1021/am300542h.
Fischer, D., Li, Y., Ahlemeyer, B., Krieglstein, J., & Kissel, T. (2003). In vitro cytotoxicity testing of polycations: Influence of polymer structure on cell viability and hemolysis. *Biomaterials, 24*(7), 1121–1131. http://dx.doi.org/10.1016/S0142-9612(02)00445-3.
Gharibi, R., Yeganeh, H., Gholami, H., & Hassan, Z. M. (2014). Aniline tetramer embedded polyurethane/siloxane membranes and their corresponding nanosilver composites as intelligent wound dressing materials. *RSC Advances, 4*(107), 62046–62060. http://dx.doi.org/10.1039/C4RA11454J.
Gharibi, R., Yeganeh, H., Rezapour-Lactoee, A., & Hassan, Z. M. (2015). Stimulation of wound healing by electroactive, antibacterial, and antioxidant Polyurethane/Siloxane dressing membranes: In vitro and in vivo evaluations. *ACS Applied Materials & Interfaces, 7*(43), 24296–24311. http://dx.doi.org/10.1021/acsami.5b08376.
Ghasemi-Mobarakeh, L., Prabhakaran, M. P., Morshed, M., Nasr-Esfahani, M.-H., & Ramakrishna, S. (2008). Electrospun poly(ε-caprolactone)/gelatin nanofibrous scaffolds for nerve tissue engineering. *Biomaterials, 29*(34), 4532–4539. http://dx.doi.org/10.1016/j.biomaterials.2008.08.007.
Harnett, E. M., Alderman, J., & Wood, T. (2007). The surface energy of various biomaterials coated with adhesion molecules used in cell culture. *Colloids and Surfaces B: Biointerfaces, 55*(1), 90–97. http://dx.doi.org/10.1016/j.colsurfb.2006.11.021.
Hassiba, A. J., El Zowalaty, M. E., Nasrallah, G. K., Webster, T. J., Luyt, A. S., Abdullah, A. M., & Elzatahry, A. A. (2016). Review of recent research on biomedical applications of electrospun polymer nanofibers for improved wound healing. *Nanomedicine, 11*(6), 715–737. http://dx.doi.org/10.2217/nnm.15.211.
Hejna, A., Formela, K., & Saeb, M. R. (2015). Processing, mechanical and thermal behavior assessments of polycaprolactone/agricultural wastes biocomposites. *Industrial Crops and Products, 76*, 725–733. http://dx.doi.org/10.1016/j.indcrop.2015.07.049.
ISO10993-5 (2009). *International organization for standardization, biological evaluation of medical devices part 5: Tests for In vitro cytotoxicity*, *Vol. 5*, 32. Retrieved from https://www.iso.org/standard/36406.html.
Ignatova, M., Manolova, N., & Rashkov, I. (2007). Novel antibacterial fibers of quaternized chitosan and poly(vinyl pyrrolidone) prepared by electrospinning. *European Polymer Journal, 43*(4), 1112–1122. http://dx.doi.org/10.1016/j.eurpolymj.2007.01.012.
Ignatova, M. G., Manolova, N. E., Toshkova, R. A., Rashkov, I. B., Gardeva, E. G., Yossifova, L. S., & Alexandrov, M. T. (2010). Electrospun nanofibrous mats containing quaternized chitosan and polylactide with in vitro antitumor activity against HeLa cells. *Biomacromolecules, 11*(6), 1633–1645. http://dx.doi.org/10.1021/bm100285n.
Jussila, J., Leppäniemi, A., Paronen, M., & Kulomäki, E. (2005). Ballistic skin simulant. *Forensic Science International, 150*(1), 63–71. http://dx.doi.org/10.1016/j.forsciint.2004.06.039.
Kalluri, R., & Zeisberg, M. (2006). Fibroblasts in cancer. *Nat Rev Cancer, 6*(5), 392–401. http://dx.doi.org/10.1038/nrc1877 Retrieved from.
Khan, R. A., Beck, S., Dussault, D., Salmieri, S., Bouchard, J., & Lacroix, M. (2013). Mechanical and barrier properties of nanocrystalline cellulose reinforced poly(caprolactone) composites: Effect of gamma radiation. *Journal of Applied Polymer Science, 129*(5), 3038–3046. http://dx.doi.org/10.1002/app.38896.
Labet, M., & Thielemans, W. (2009). Synthesis of polycaprolactone: A review. *Chemical Society Reviews, 38*(12), 3484–3504. http://dx.doi.org/10.1039/B820162P.
Liakos, I., Rizzello, L., Hajiali, H., Brunetti, V., Carzino, R., Pompa, P. P., ... Mele, E. (2015). Fibrous wound dressings encapsulating essential oils as natural antimicrobial agents. *Journal of Materials Chemistry B, 3*(8), 1583–1589. http://dx.doi.org/10.1039/C4TB01974A.
Liang, D., Lu, Z., Yang, H., Gao, J., & Chen, R. (2016). Novel asymmetric wettable AgNPs/chitosan wound dressing: In vitro and In vivo evaluation. *ACS Applied Materials & Interfaces, 8*(6), 3958–3968. http://dx.doi.org/10.1021/acsami.5b11160.
MacNeil, S. (2007). Progress and opportunities for tissue-engineered skin. *Nature, 445*(7130), 874–880. http://dx.doi.org/10.1038/nature05664 Retrieved from.
Mele, E. (2016). Electrospinning of natural polymers for advanced wound care: Towards responsive and adaptive dressings. *Journal of Materials Chemistry B, 4*(28), 4801–4812. http://dx.doi.org/10.1039/C6TB00804F.
Neamnark, A., Sanchavanakit, N., Pavasant, P., Bunaprasert, T., Supaphol, P., & Rujiravanit, R. (2007). In vitro biocompatibility evaluations of hexanoyl chitosan film. *Carbohydrate Polymers, 68*(1), 166–172. http://dx.doi.org/10.1016/j.carbpol.2006.07.024.
Ninan, N., Forget, A., Shastri, V. P., Voelcker, N. H., & Blencowe, A. (2016). Antibacterial and anti-inflammatory pH-responsive tannic acid-carboxylated agarose composite hydrogels for wound healing. *ACS Applied Materials & Interfaces, 8*(42), 28511–28521. http://dx.doi.org/10.1021/acsami.6b10491.
Niyonsaba, F., & Ogawa, H. (2005). Protective roles of the skin against infection: Implication of naturally occurring human antimicrobial agents β-defensins, cathelicidin LL-37 and lysozyme. *Journal of Dermatological Science, 40*(3), 157–168. http://dx.doi.org/10.1016/j.jdermsci.2005.07.009.
Pailler-Mattei, C., Bec, S., & Zahouani, H. (2008). In vivo measurements of the elastic mechanical properties of human skin by indentation tests. *Medical Engineering & Physics, 30*(5), 599–606. http://dx.doi.org/10.1016/j.medengphy.2007.06.011.
Prado, H. J., & Matulewicz, M. C. (2014). Cationization of polysaccharides: A path to greener derivatives with many industrial applications. *European Polymer Journal, 52*(1), 53–75. Retrieved from http://www.scopus.com/inward/record.url?eid=2-s2.0-84892573985&partnerID=40&md5=d1dc726f0b175319abb38dbe841c6f97.
Rieger, K. A., Birch, N. P., & Schiffman, J. D. (2013). Designing electrospun nanofiber mats to promote wound healing – A review. *Journal of Materials Chemistry B, 1*(36), 4531–4541. http://dx.doi.org/10.1039/C3TB20795A.
Rinaudo, M., Milas, M., & Le Dung, P. (1993). Characterization of chitosan. Influence of ionic strength and degree of acetylation on chain expansion. *International Journal of Biological Macromolecules, 15*(5), 281–285. http://dx.doi.org/10.1016/0141-8130(93)90027-J.
Rojo, E., Peresin, M. S., Sampson, W. W., Hoeger, I. C., Vartiainen, J., Laine, J., & Rojas, O. J. (2015). Comprehensive elucidation of the effect of residual lignin on the physical, barrier, mechanical and surface properties of nanocellulose films. *Green Chemistry, 17*(3), 1853–1866. http://dx.doi.org/10.1039/C4GC02398F.
dos Santos, D. M., de Bukzem, A. L., & Campana-Filho, S. P. (2016). Response surface methodology applied to the study of the microwave-assisted synthesis of quaternized chitosan. *Carbohydrate Polymers, 138*, 317–326. http://dx.doi.org/10.1016/j.carbpol.2015.11.056.
Shevchenko, R. V., James, S. L., & James, S. E. (2009). A review of tissue-engineered skin bioconstructs available for skin reconstruction. *Journal of The Royal Society Interface, 7*(43), 229. [LP-258. Retrieved from] http://rsif.royalsocietypublishing.org/content/7/43/229.abstract.
Song, D. W., Kim, S. H., Kim, H. H., Lee, K. H., Ki, C. S., & Park, Y. H. (2016). Multi-biofunction of antimicrobial peptide-immobilized silk fibroin nanofiber membrane: Implications for wound healing. *Acta Biomaterialia, 39*, 146–155. http://dx.doi.org/10.1016/j.actbio.2016.05.008.
Sonia, T. A., & Sharma, C. P. (2011). In vitro evaluation of N-(2-hydroxy) propyl-3-trimethyl ammonium chitosan for oral insulin delivery. *Carbohydrate Polymers, 84*(1), 103–109. http://dx.doi.org/10.1016/j.carbpol.2010.10.070.
Sugihara, T., Ohura, T., Homma, K., & Igawa, H. H. (1991). The extensibility in human skin: Variation according to age and site. *British Journal of Plastic Surgery, 44*(6), 418–422. http://dx.doi.org/10.1016/0007-1226(91)90199-T.
van Oss, C. J. (1995). Hydrophobicity of biosurfaces — Origin, quantitative determination and interaction energies. *Colloids and Surfaces B: Biointerfaces, 5*(3), 91–110. http://dx.doi.org/10.1016/0927-7765(95)01217-7.
Van Oss, C. J., Chaudhury, M. K., & Good, R. J. (1988). Interfacial Lifshitz-van der Waals and polar interactions in macroscopic systems. *Chemical Reviews, 88*(6), 927–941. http://dx.doi.org/10.1021/cr00088a006.
Verheul, R. J., Amidi, M., van Steenbergen, M. J., van Riet, E., Jiskoot, W., & Hennink, W. E. (2009). Influence of the degree of acetylation on the enzymatic degradation and in vitro biological properties of trimethylated chitosans. *Biomaterials, 30*(18), 3129–3135. http://dx.doi.org/10.1016/j.biomaterials.2009.03.013.
Verlee, A., Mincke, S., & Stevens, C. V. (2017). Recent developments in antibacterial and antifungal chitosan and its derivatives. *Carbohydrate Polymers, 164*, 268–283. http://dx.doi.org/10.1016/j.carbpol.2017.02.001.
Werner, S., Krieg, T., & Smola, H. (2007). Keratinocyte-fibroblast interactions in wound healing. *Journal of Investigative Dermatology, 127*(5), 998–1008. http://dx.doi.org/10.1038/sj.jid.5700786.
Wongwanakul, R., Jianmongkol, S., Gonil, P., Sajomsang, W., Maniratanachote, R., & Auewiriyavit, S. (2017). Biocompatibility study of quaternized chitosan on the proliferation and differentiation of Caco-2 cells as an in vitro model of the intestinal barrier. *Journal of Bioactive and Compatible Polymers, 32*(1), 92–107. http://dx.doi.org/10.1177/0883911516658780.
Woodruff, M. A., & Hutmacher, D. W. (2010). The return of a forgotten polymer—Polycaprolactone in the 21st century. *Progress in Polymer Science, 35*(10), 1217–1256. http://dx.doi.org/10.1016/j.progpolymsci.2010.04.002.
Xu, Y., Du, Y., Huang, R., & Gao, L. (2003). Preparation and modification of N-(2-hydroxyl) propyl-3-trimethyl ammonium chitosan chloride nanoparticle as a protein carrier. *Biomaterials, 24*(27), 5015–5022. http://dx.doi.org/10.1016/S0142-9612(03)00408-3.
Xu, R., Xia, H., He, W., Li, Z., Zhao, J., Liu, B., ... Wu, J. (2016). Controlled water vapor transmission rate promotes wound-healing via wound re-epithelialization and contraction enhancement. *Scientific Reports, 6*, 24596. http://dx.doi.org/10.1038/srep24596 Retrieved from.
Yevlampieva, N. P., Gubarev, A. S., Gorshkova, M. Y., Okrugin, B. M., & Ryumtsev, E. I. (2015). Hydrodynamic behavior of quaternized chitosan at acidic and neutral pH. *Journal of Polymer Research, 22*(9), 1–9. http://dx.doi.org/10.1007/s10965-015-0802-7.
Yoo, H.-J., & Kim, H.-D. (2008). Synthesis and properties of waterborne polyurethane hydrogels for wound healing dressings. *Journal of Biomedical Materials Research Part B: Applied Biomaterials, 85B*(2), 326–333. http://dx.doi.org/10.1002/jbm.b.30950.